Structures 56 (2023) 104844

Contents lists available at ScienceDirect

Structures

journal homepage: www.elsevier.com/locate/structures

A new approach to the stability design of Ramberg–Osgood material struts

Anton Köllner [a,*], Leroy Gardner [b], M. Ahmer Wadee [b,*]

[a] Institute of Mechanics, Stability and Failure of Functionally Optimized Structures Group, Technische Universität Berlin, Einsteinufer 5, 10587, Berlin, Germany
[b] Department of Civil and Environmental Engineering, Imperial College London, London SW7 2AZ, United Kingdom

ARTICLE INFO

Keywords:
Ramberg–Osgood nonlinearity
Energy method
Column strength
Flexural buckling
Design
Stainless steel
Cold-formed steel
Aluminium alloys

ABSTRACT

An energy formulation employing total potential energy principles is presented to derive a governing equation for strength predictions of struts made from materials following the Ramberg–Osgood constitutive law such as stainless steel, cold-formed steel, and aluminium alloys. The formula is generic and applicable to arbitrary cross-sections and all strut slendernesses for which flexural buckling is critical. Extensive comparisons against experimental data on square and rectangular hollow section struts as well as finite element simulations demonstrate the accuracy of the developed formula, while the effect of varying material parameters is examined through comprehensive parametric studies. Owing to its simplicity and its derivation based on mechanical principles, arbitrary configurations of material parameters and cross-sections can be analysed, making the formula suitable for use in design practice, representing effectively a non-iterative alternative to the widely accepted design load employing the tangent modulus. With the aid of the formula, new column buckling design provisions are developed, which show excellent agreement with experimental data and meet the reliability requirements specified within the structural Eurocodes.

1. Introduction

Structural instability plays a pivotal role in the design of structural members resisting compression [1], where such members may be referred to as struts or columns. In design practice (*e.g.* [2,3]), the strength of struts is typically evaluated against the normalized strut slenderness, a non-dimensional quantity comprising the ratio of the squash load to the Euler buckling load, and refers to the maximum load that the strut can withstand, *i.e.* the 'ultimate strength'. Considering linear elastic, perfectly plastic material behaviour, design curves derived from mechanical principles are well-established, *e.g.* the Perry–Robertson formula, where first yield in a compressed imperfect strut defines failure [4]. Regions of normalized slendernesses associated with geometric instability (buckling) and material failure (yielding) are well-defined for perfect systems, and the combined effects of geometric imperfections and residual stresses are considered through an imperfection factor. Design formulae have been calibrated with reference to extensive experimental evidence and provide a sound basis for ultimate strength predictions [5–8].

This is different when structural members exhibit a rounded constitutive response, where widely used materials such as stainless steel, cold-formed steel and aluminium alloys are frequently modelled using the well-established Ramberg–Osgood law [9–11]. The Ramberg–Osgood law provides an empirical, non-invertible, nonlinear strain–stress relationship. Despite its benefits in representing the constitutive behaviour of the aforementioned materials adequately, its specific character makes any attempt at deriving non-empirical governing equations for determining the strength of structural members challenging. Design curves and formulae are predominantly developed empirically, being based on finite element analyses and experimental investigations [12–14]. The 'tangent modulus approach' may be considered as an exception in this context, which is generally implemented for obtaining buckling loads as well as describing the post-buckling behaviour of struts made from a material with a Ramberg–Osgood-type nonlinearity [15–18]. The tangent modulus buckling load is also used in the American design specification for cold-formed stainless steel structures [3]; however, all works considering this approach require an iterative solution scheme for which the current work aims to render superfluous, thus providing an alternative to current approaches. In contrast, empirical approaches based on numerical studies are present in the Australian/New Zealand standard for structural stainless steel [19], where the method developed in [12] is implemented.

The current work addresses the aforementioned issue by deriving a governing equation to determine the buckling load of struts readily considering the Ramberg–Osgood nonlinearity. A total potential energy formulation is employed alongside expressing deformation measures by associated linear parts by means of an incremental coordinate approach [20,21]. As a consequence, considering configurations for which

* Corresponding authors.
E-mail addresses: anton.koellner@tu-berlin.de (A. Köllner), leroy.gardner@imperial.ac.uk (L. Gardner), a.wadee@imperial.ac.uk (M.A. Wadee).

https://doi.org/10.1016/j.istruc.2023.07.034
Received 28 March 2023; Received in revised form 23 June 2023; Accepted 4 July 2023
Available online 18 July 2023

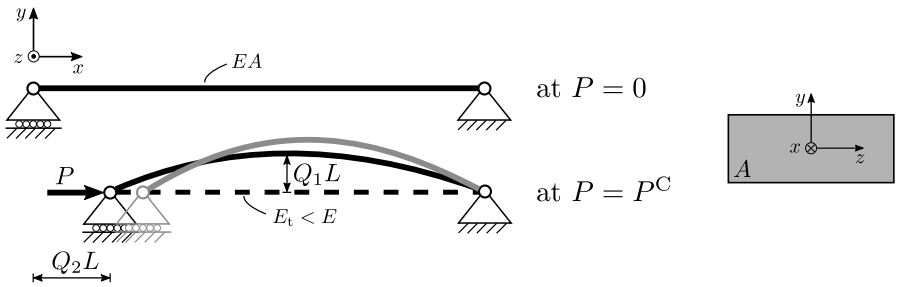

Fig. 1. Geometric model of the strut; buckling displacement associated with linear and nonlinear material behaviour is illustrated by black and grey respectively, with E being the initial elastic modulus, E_t being the tangent modulus and A being the cross-sectional area (arbitrary, so long as flexural buckling is critical); note that presently the weaker flexural axis is assigned to be the z-axis.

flexural buckling is deemed to be the dominant failure mechanism, the current work presents a formula based on fundamental mechanical principles suitable for design practice, effectively proposing a non-iterative alternative to the tangent modulus approach. With the derived formula, a detailed investigation of the effect of varying material parameters on the strength predictions is conducted. The work highlights that design guidelines employing fixed empirical quantities (*e.g.* Eurocode 3) do not cover the band of strength predictions associated with changing material parameters for intermediate and small normalized slendernesses. In contrast, guidelines related to the tangent modulus approach can tend to overestimate the column strength for large normalized slendernesses. A new design provision is proposed that employs the derived formula alongside a correction factor yielding excellent agreement with experimental data for all configurations where flexural buckling is critical.

In the subsequent exposition, the total potential energy formulation and the buckling analysis are described in Sections 2 and 3 respectively. A comprehensive parametric study on the strength of struts with Ramberg–Osgood materials is presented in Section 4. This study includes extensive comparisons against existing experimental data and finite element simulations, which are employed to propose a novel design provision that is assessed using a structural reliability analysis. Conclusions are drawn in Section 5.

2. Energy formulation

In contrast with total potential energy formulations for studying the buckling of struts made from a material obeying linear elasticity, nonlinear material behaviour requires the consideration of axial deformations in the pre-buckling state, *i.e.* on the non-trivial fundamental equilibrium path, since the material tangent modulus E_t changes before the instability is triggered (see Fig. 1).

In the following exposition, energy contributions associated with stretching and bending deformations are separately derived. Consider the Ramberg–Osgood law (in one dimension), which is commonly used to describe the nonlinear constitutive behaviour of stainless steel, cold-formed steel and aluminium alloys, thus [9,10]:

$$\varepsilon = \frac{\sigma}{E} + \alpha_{ro}\left(\frac{\sigma}{f_y}\right)^n, \tag{1}$$

with E being the initial elastic (Young's) modulus, α_{ro} being the 0.2% offset strain, f_y being the material 0.2% proof stress, which is taken to be the equivalent of a yield stress, and n being a hardening exponent. An expression for the strain energy density $U_\rho = \int \sigma \, \mathrm{d}\varepsilon$ is readily derived by determining $\mathrm{d}\varepsilon$ from Eq. (1) and subsequent integration over σ, thus:

$$U_\rho = \frac{1}{2}\frac{\sigma^2}{E} + \frac{n\alpha_{ro}}{(n+1)f_y^n}\sigma^{n+1}. \tag{2}$$

Considering that the Ramberg–Osgood law given in Eq. (1) can be expressed in terms of linear strain contributions $\varepsilon_L = \sigma/E$, Eq. (2) can be rewritten, thus:

$$U_\rho = \frac{1}{2}E\varepsilon_L^2 + \frac{n\alpha_{ro}}{(n+1)f_y^n}E^{n+1}\varepsilon_L^{n+1} \tag{3}$$

where linear strain contributions ε_L presently serve as the deformation measure to express the strain energy; note that even though a linear strain measure is used, the expression for the energy stored in the system employing the Ramberg–Osgood law is still exact. Moreover, it is also noteworthy that for studying the flexural buckling behaviour of struts, one-dimensional descriptions, as provided in Eqs. (1)–(3), are sufficient. Two-dimensional deformations, as for instance required for local buckling responses, can be considered as described in [22].

Expressions for linear strains ε_L are obtained by employing geometric concepts used to model the buckling behaviour of simply-supported struts. The linear part of the buckling displacement w_L is assumed to be identical to the lowest linear eigenmode for a simply-supported strut made from a linear elastic material, thus:

$$w_L = Q_1 L \sin\left(\frac{\pi x}{L}\right), \tag{4}$$

where Q_1 is the normalized amplitude of the linear buckling displacement as illustrated in Fig. 1. To visualize the concept of describing nonlinear deformation by linear quantities, Fig. 1 depicts the actual buckling displacement in grey corresponding to the overall nonlinear deformation that, however, is associated with and thus expressed by means of the linear deformation shown in black. Note that in the present context, linear and nonlinear strictly refers to the material behaviour rather than the geometric nonlinearity which is usually associated with buckling.

For bending deformations, the assumptions as presented in [22] are employed assuming that both linear and total bending strains follow Euler–Bernoulli beam relationships, so that plane sections remain plane and perpendicular to the neutral axis of bending (*cf.* [22]). Thus, linear bending strains are given by the well-known relationship for small curvatures:

$$\varepsilon_L^b = -y\frac{\partial^2 w_L}{\partial x^2}. \tag{5}$$

The linear in-plane shortening of the strut u_L is expressed by (*cf.* [21]):

$$u_L = Q_2 L - \frac{1}{2}\int_L \left(\frac{\partial w_L}{\partial x}\right)^2 \mathrm{d}x, \tag{6}$$

where $Q_2 L$ is the total linear end-shortening of the strut (with Q_2 itself representing the corresponding linear strain measure, see Fig. 1) and the second term represents inextensional shortening due to the buckling displacement [21,23]. Note that Eq. (6) employs the assumption that strains along the neutral axis are constant which represents an accurate approximation for strut buckling problems without excessively large post-buckling deflections, thus effectively providing an averaged in-plane strain in the form of $\varepsilon_L^0 = u_L/L$ [21].

Stretching and bending energy contributions are obtained by inserting linear in-plane/membrane strains (ε_L^0) and linear bending strains (ε_L^b) respectively into Eq. (3) and integrating over the volume of the strut. An analytical expression can be obtained for both energy contributions. The stretching energy (U_s) of a strut with the cross-sectional

area A obeying the Ramberg–Osgood law is given thus:

$$U_s = EAL\left(Q_2 - \frac{\pi^2 Q_1^2}{4}\right)^2\left[\frac{1}{2} + c_1\left(Q_2 - \frac{\pi^2 Q_1^2}{4}\right)^{n-1}\right], \tag{7}$$

where:

$$c_1 = \frac{n\alpha_{ro}E^n}{(n+1)f_y^n}, \tag{8}$$

and the bending energy (U_b) is given thus:

$$U_b = \frac{\pi^4 EI_{zz}}{4L}Q_1^2 + c_0\frac{c_1\pi^{2n+3/2}EI_{zz}^*}{L^n}Q_1^{n+1}, \tag{9}$$

with $I_{zz} = \int_A y^2\,dA$, $I_{zz}^* = \int_A y^{n+1}\,dA$ and $c_0 = \Gamma\left[1+\frac{n}{2}\right]/\Gamma\left[\frac{3+n}{2}\right]$. The Gamma-function $\Gamma[n]$ is used to provide a general solution for integrating expressions such as $[\sin(mx)]^{n+1}$ with an arbitrary hardening parameter n with $n \geq 1$. Note that for specific n, the integral can also be evaluated using integration by parts.

The potential of the applied force P is given by

$$\Phi = -P\Delta, \tag{10}$$

where:

$$\Delta = \left[Q_2 + \alpha_{ro}\left(\frac{E}{f_y}\right)^n Q_2^n\right]L = \left[Q_2 + \left(\frac{n+1}{n}\right)c_1 Q_2^n\right]L, \tag{11}$$

which comprises both linear and nonlinear parts of the total end-shortening of the strut. With Eqs. (7)–(11), the total potential energy of the strut can be obtained, thus:

$$V = U_s + U_b + \Phi. \tag{12}$$

Note that the total potential energy is expressed in terms of the generalized coordinates Q_1 and Q_2, *i.e.* $V = V(Q_1, Q_2, P)$, which represent linear parts of respective deformations such as buckling displacement and end-shortening.

3. Buckling analysis

To derive the buckling load of struts made from materials obeying a Ramberg–Osgood type nonlinearity, an incremental coordinate approach is employed (*cf.* [21]), making use of the coordinate transformation:

$$Q_1 = q_1 \quad \text{and} \quad Q_2 = \frac{P}{EA} + q_2, \tag{13}$$

where q_2 represents an increment in linear axial strain relative to the linear axial compressive strain $P/(EA)$ and q_1 is introduced for notation consistency. With the change in coordinates, deformation states relative to the non-trivial fundamental path are considered instead of the unloaded configuration. Note also that despite the fundamental path being nonlinear, its linear part is expressed by $P/(EA)$, which represents the linear end-shortening of the strut prior to buckling.

Employing the change in coordinates enables a straightforward derivation of the buckling load since the fundamental path of the nonlinear strut is now characterized by q_1 and q_2 being zero; of course this characterization is strictly correct for a perfect strut. It should be stressed that q_1 and q_2 still represent linear contributions to buckling displacement and end-shortening respectively. Substituting Eq. (13) into Eq. (12), using the dimensionless parameter p, defined as $P/(EA)$, gives an updated total potential energy, *i.e.* $V = V(q_1, q_2, p)$, thus:

$$\begin{aligned} V = {} & EAL\left(p + q_2 - \frac{\pi^2 q_1^2}{4}\right)^2\left[\frac{1}{2} + c_1\left(p + q_2 - \frac{\pi^2 q_1^2}{4}\right)^{n-1}\right] \\ & + \frac{\pi^4 EI_{yy}}{4L}q_1^2 + c_0\frac{c_1\pi^{2n+3/2}EI_{zz}^*}{L^n}q_1^{n+1} \\ & - EALp\left[p + q_2 + \left(\frac{n+1}{n}\right)c_1\left(p+q_2\right)^n\right]. \end{aligned} \tag{14}$$

The buckling loads of Ramberg–Osgood struts can now be directly determined implementing the criticality condition at the fundamental (nonlinear) path described by $q_1 = q_2 = 0$, where stability is lost whenever the Hessian of V, *i.e.* $V_{ij} \equiv \partial^2 V/\partial q_i \partial q_j$, becomes singular [20], thus:

$$\det\left(V_{ij}^C\Big|_{\substack{q_1=0\\q_2=0}}\right) = V_{11}^C V_{22}^C = 0. \tag{15}$$

In Eq. (15), coefficients $V_{12}^C = V_{21}^C$ vanish on the fundamental path and terms $(\bullet)^C$ refer to the evaluation at the critical state where $q_1 = q_2 = 0$. Note that subscript numerals refer to partial derivatives with respect to the generalized coordinates q_1 and q_2. The condition $V_{11}^C = 0$ gives the buckling load for Ramberg–Osgood material struts. Note that the condition $V_{22}^C = 0$, which could have potentially provided an additional buckling load, turns out to be irrelevant in evaluating the buckling behaviour. After some algebraic manipulation the condition $V_{11}^C = 0$ can be written in the following form:

$$\begin{aligned} V_{11}^C \equiv \frac{\partial^2 V}{\partial q_1^2}\bigg|^C &= f(p) = p^n + C_1 p + C_2 = 0, \\ \text{with:}\quad C_1 &= \frac{1}{(n+1)c_1}, \quad C_2 = -\frac{c_2}{c_1}, \quad c_2 = \frac{\pi^2 I_{zz}}{(n+1)AL^2}, \end{aligned} \tag{16}$$

where c_1 was provided in Eq. (8). The expression presented in Eq. (16) is the governing equation for the global flexural buckling load of Ramberg–Osgood struts, with its solution providing the buckling load P^C:

$$f(p) = 0 \Longrightarrow p^C = p^C(E, n, f_y, \lambda), \quad \text{with} \quad P^C = p^C EA, \tag{17}$$

where the strut slenderness $\lambda = L/r_{zz}$ (r_{zz} is the radius of gyration about the weaker flexural axis of the cross-section of the strut, defined thus: $r_{zz}^2 = I_{zz}/A$) can be introduced by replacing the length of the strut with $L = \lambda\sqrt{I_{zz}/A}$ (or its corresponding buckling effective length L_e for boundary conditions other than simply-supported), providing an expression depending on the material parameters (E, n, f_y) and the slenderness only. Analytical (closed-form) solutions can be obtained for $n = 3$, which converts Eq. (17) into a cubic polynomial equation (see Appendix); however, for $n > 3$ (n being the hardening parameter) solutions are readily obtained by simple numerical methods or built-in root evaluations in algebraic manipulation software tools or spreadsheet software.

Since the current work focuses on determining the critical buckling load, the effect of elastic unloading (with the elastic modulus E) once buckling occurs does not need to be incorporated within the energy formulation (for instance, as in the Shanley model [24,25]). The solution obtained from Eq. (17) – as will be demonstrated in Section 4 – is equivalent to the tangent modulus load and thus corresponds to the lowest possible bifurcation load. It should be stressed that for evaluating flexural buckling, the analytical expressions provided in Eqs. (16) and (17) are entirely generic and thus applicable to any cross-sections with arbitrary material parameters. Imperfections are not considered within the present energy formulation. Corresponding reductions in ultimate strength are considered in the development of the design model in Section 4.5 by introducing a correction factor.

4. Results

In the current section, predictions of the buckling load using the solution to Eq. (17) are compared against results obtained by finite element simulations first. Subsequently, a detailed comparison against experimental results and Eurocode 3 (EC3) predictions is provided, followed by a direct comparison against predictions using the tangent modulus load. Results from a parametric study of varying material parameters are provided. At the end of the section, a novel design provision is presented and a reliability analysis is performed.

4.1. Comparison against finite element simulations

Finite element (FE) simulations were conducted within the commercial software ABAQUS [26], where nonlinear analyses of imperfect struts were executed. Since it is the motivation of this comparison to verify the newly developed buckling load formula (see Eqs. (16) and (17)), imperfections were introduced as perturbations of eigenforms from corresponding linear buckling analyses (LBA) with their magnitude being set to be as small as possible to limit their effects on the critical load, typically ranging between $L/10000$ and $L/20000$.[1] The built-in material option "Deformation plasticity" representing Ramberg–Osgood-like behaviour as implemented in the energy formulation (see Section 2) was selected in the FE analyses. In the comparison with the FE analyses, material parameters representing an aluminium alloy have been used with the initial Young's modulus and the yield strength being $E = 70\,\text{GPa}$ and $f_y = 220\,\text{MPa}$ respectively. The hardening exponent n was considered to vary over a considerably large range, as indicated in Fig. 2, which is deemed to cover a majority of typical materials.

The results presented throughout the work are provided in terms of the normalized slenderness $\bar{\lambda} = \sqrt{P_y/P_E}$ as defined in Eurocode 3, with $P_y = Af_y$ being the squash load and A being the area of the cross-section (or an effective area $A = A_{\text{eff}}$ for class 4 cross-sections, see [2,27]) and P_E is the Euler (buckling) load of a strut made from a linear elastic material. The analyses employing the proposed formula (see Eq. (16)) are independent of cross-section geometry so long as flexural buckling is critical. Therefore, in the comparative study against FE simulations, a simple solid 1 mm × 1 mm square cross-section is chosen where lengths are varied to represent all normalized slendernesses of interest.

Fig. 2 shows the buckling curves in terms of the strength reduction factor $\chi = P_u/P_y$ against normalized slenderness $\bar{\lambda}$ for hardening parameters $n = \{3, 7, 11, 15, 19\}$, where for the current model the ultimate load P_u is considered to be equal to the critical buckling load P^C. Results are provided for normalized slendernesses ranging from 0.2 to 3.0 with the lower bound corresponding to the buckling load being equal to the squash load, thus: $\chi = 1$. Corresponding results from FE analyses are visualized using symbols ∘, □, ◇, ▽ and △, respectively. The buckling curve associated with Euler buckling, *i.e.* buckling loads of a strut made from a linear elastic material, is also provided in Fig. 2 through a dashed line. As can be seen in Fig. 2, results obtained for the current model and FE analyses practically coincide verifying the proposed energy formulation, where negligible deviations are attributed to the small perturbations in the FE analyses.

The effect of material nonlinearity is clearly highlighted in Fig. 2. All curves essentially follow the behaviour of linear elasticity for normalized slenderness larger than $\bar{\lambda} = 2.5$. For $\bar{\lambda} < 2.5$, with the increasing hardening parameter n, the buckling curves follow the linear elastic curve up to smaller normalized slenderness values. Whereas for $n = 3$ the curves already deviate for $\bar{\lambda} < 2.5$, this measure decreases to approximately 1.6 for $n = 7$ and appears to converge to a normalized slenderness of approximately 1.2 for very high values of n (*e.g.* see the curves for $n = 15$ and $n = 19$ in Fig. 2). Note that this effect relates to the tangent stiffness remaining closer to the initial (linear) stiffness for larger ranges of applied stress with increasing n.

A second phenomenon is highlighted in Fig. 2 which occurs particularly for $n > 3$. Considering the response for smaller $\bar{\lambda}$, unlike the qualitative behaviour that appears to be similar between the linear elastic case and $n = 3$, the curves for $n > 3$ show a characteristic change where once the curves deviate from the linear elastic response, larger n values cause decreasing slopes resulting in the curves intersecting each other at $\bar{\lambda} \approx 0.55$. As a consequence, larger hardening parameters n result in buckling loads reaching the corresponding squash load at smaller $\bar{\lambda}$ values; thus $\chi = 1$ is reached for $n = 3$ at $\bar{\lambda} \approx 0.6$, but for larger n values corresponding normalized slendernesses appear to converge towards 0.25.

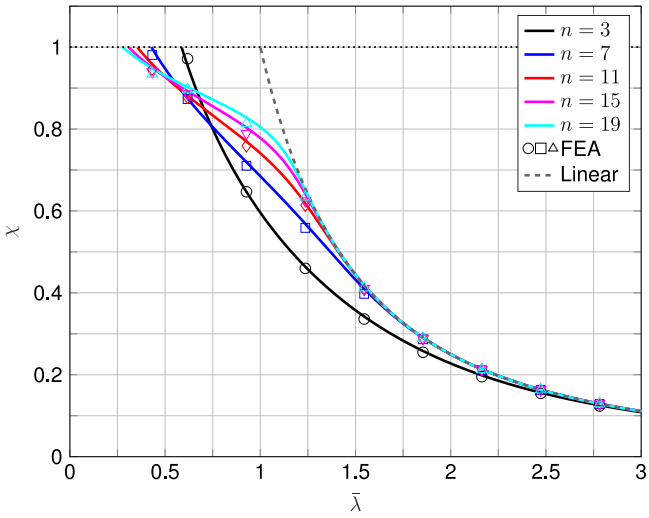

Fig. 2. Strength reduction factor χ vs. normalized slenderness $\bar{\lambda}$ for various hardening parameters n with $E = 70$ GPa and $f_y = 220$ MPa; $\chi = 1$ is denoted as the 'squash' strength.

4.2. Comparison against experiments and Eurocode 3

With the energy formulation having been verified by FE modelling, comparisons against experimental data published in the literature and design codes are provided next. Results from experiments for the ultimate strength of square (SHS) and rectangular (RHS) hollow section struts documented in the literature [13,28,29] are considered. The studies cover different types or grades of stainless steel (*e.g.* ferritic, lean duplex) and cross-section properties. Information about the material parameters and geometry provided in the respective works are considered for the corresponding load predictions alongside the calculation of the normalized slenderness. The results of all tests and corresponding predictions of the current model are presented in Fig. 3 in terms of the strength reduction factor χ versus the normalized slenderness $\bar{\lambda}$. Experimental data are visualized by symbols △, ∘, and □, from Refs. [13,28,29] respectively, where corresponding model predictions are provided by filled symbols. The results are summarized in Table 1 alongside the respective material and geometric parameters.

In addition to the comparison between experiments and model predictions, Fig. 3 also shows the design curves from Eurocode 3 Part 1.4 (solid line) [2], with parameters α and $\bar{\lambda}_0$ set as 0.49 and 0.40 respectively (as recommended for cold-formed stainless steels), and as an example, a curve corresponding to the SEI/ASCE-8 standard (dotted line) with $n = 8.6$ (as considered in [29]; normally single points would be required for the respective material parameters) to highlight a general observation to be discussed subsequently. The Euler buckling curve (dashed line; for linear elastic behaviour) is also provided in Fig. 3 for reference.

Fig. 3 indicates good agreement between the model, experiments and design predictions for normalized slendernesses between 0.4 and 1.0. For $\bar{\lambda} > 1.0$, a larger (relative) scatter between the model predictions, experiments and design predictions is observed, where the behaviour of the model appears to be in agreement with the SEI/ASCE-8 design code indicated by the dotted line in Fig. 3. For $\bar{\lambda} > 1.5$,

[1] Note that buckling loads of nonlinear materials cannot be obtained through performing LBA in FE simulations. An alternative method to the one used would be to introduce an initial step preloading the column before running a buckling analysis. However, this requires an iterative procedure to find adequate preloads which was deemed to make an efficient implementation more cumbersome.

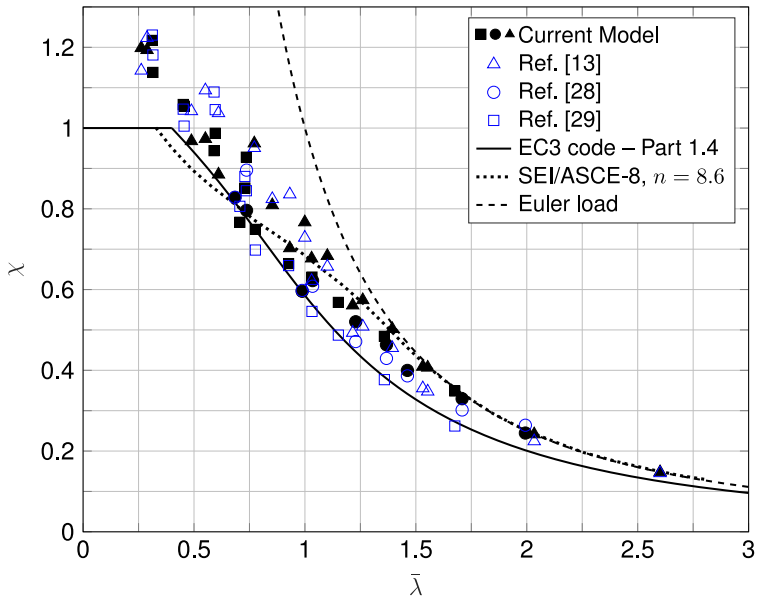

Fig. 3. Comparison against experimental data from Table 1; strength reduction factor χ vs. normalized slenderness $\bar{\lambda}$ for stainless steel with material and geometric parameters taken from experiments. For individual comparisons, the reader is advised to compare the open and filled symbols at identical $\bar{\lambda}$ values.

Table 1
Comparisons of model (mod) results against experimental (exp) data and Eurocode (EC3).

Refs.	Material parameters			Dimensions (mm)			Results				
	E (GPa)	f_y (MPa)	n	Length	Height	Width	$\bar{\lambda}$	P^C_{mod} (kN)	$P_{u,exp}$ (kN)	$P_{u,exp}/P^C_{mod}$	χ_{EC3}/χ_{mod}
[13]	198.00	683	7	310.0	50.0	30.0	0.49	240.7	259.2	1.08	0.98
				660.0	50.1	30.1	1.03	168.0	154.2	0.92	0.83
				1010.0	50.5	30.2	1.55	99.9	85.4	0.85	0.76
				1310.0	50.1	30.2	2.03	59.5	55.3	0.93	0.81
				1660.0	50.4	30.1	2.60	36.8	36.2	0.98	0.85
[13]	198.00	635	6	310.0	50.3	49.7	0.29	346.6	355.3	1.03	0.84
				660.0	50.1	49.6	0.61	257.8	302.1	1.17	0.98
				1010.0	50.3	49.8	0.93	204.1	242.8	1.19	0.90
				1310.0	50.2	50.0	1.21	166.2	146.1	0.88	0.81
				1660.0	50.3	50.0	1.53	119.5	103.9	0.87	0.77
[13]	194.00	613	8	310.0	70.4	50.5	0.26	391.3	373.1	0.95	0.83
				660.0	70.7	51.0	0.55	314.0	352.8	1.12	0.93
				1010.0	70.5	50.7	0.85	265.7	270.7	1.02	0.85
				1310.0	70.4	50.7	1.10	219.7	211.2	0.96	0.76
				1660.0	70.5	50.8	1.39	163.6	148.3	0.91	0.73
[13]	194.00	610	5	1010.0	50.5	50.5	0.77	122.3	120.8	0.99	0.78
				1310.0	50.5	50.4	1.00	97.1	92.3	0.95	0.76
				1660.0	50.8	50.7	1.26	73.8	65.4	0.89	0.75
[28]	197.2	657	4.7	1199.5	79.6	79.5	0.73	597.7	672.5	1.13	0.98
				1999.0	79.6	79.5	1.22	399.6	361.9	0.91	0.86
[28]	206.4	711	5.0	799.0	60.0	60.0	0.68	445.7	445.9	1.00	0.99
				1199.0	60.0	60.0	1.03	334.4	326.9	0.98	0.90
				1599.0	59.6	60.0	1.36	249.9	231.7	0.93	0.82
				1999.0	60.0	60.0	1.70	177.2	162.3	0.92	0.80
[28]	204.00	607	4.6	797.2	39.5	79.4	0.99	365.3	366.6	1.00	1.00
				1199.0	40.0	79.2	1.46	245.7	237.4	0.97	0.85
				1600.0	39.0	79.2	1.99	148.7	160.4	1.08	0.83
[29]	211.15	404	5.8	1100.0	120.0	79.9	0.31	458.0	463	1.01	0.82
				1600.0	120.0	79.9	0.45	386.2	382	0.99	0.92
				2100.0	120.0	79.8	0.59	338.8	391	1.15	0.93
				2600.0	119.7	79.8	0.73	298.0	308	1.03	0.92
[29]	216	423	10.2	1100.0	120.0	79.9	0.31	446.0	463	1.04	0.88
				1600.0	120.0	79.9	0.46	400.8	382	0.95	0.92
				2100.0	120.0	79.8	0.60	369.2	391	1.06	0.89
				2600.0	119.7	79.8	0.74	338.3	308	0.91	0.84
[29]	211.25	404	6.3	1600.0	80.1	80.0	0.71	259.6	273	1.05	1.04
				2100.0	80.0	79.8	0.93	223.7	222	0.99	0.96
				2600.0	80.1	79.8	1.15	191.3	164	0.86	0.86
[29]	215.13	483	6.3	1100.0	60.4	60.4	0.78	229.7	214	0.93	1.00
				1600.0	60.6	60.5	1.03	191.8	166	0.87	0.89
				2100.0	60.5	60.4	1.36	149.0	116	0.78	0.79
				2600.0	60.6	60.6	1.68	109.1	82	0.75	0.78

Table 2
Mean and coefficient of variation (COV) comparing model (mod) results against experiments (exp) and the Eurocode 3 (EC3).

Normalized	exp/mod		EC3/mod		exp/EC3	
slenderness $\bar{\lambda}$	Mean	COV	Mean	COV	Mean	COV
All	0.975	0.101	0.867	0.092	1.128	0.087
$\bar{\lambda} \leq 1$	1.033	0.075	0.910	0.082	1.139	0.088
$\bar{\lambda} > 1$	0.906	0.082	0.814	0.059	1.115	0.086

the model predictions slowly converge onto the Euler buckling curve (approximately at a normalized slenderness of 1.6), where experimental results and the Eurocode show slightly smaller loads.

The direct numerical comparisons between the results obtained by the model ('mod'), experiments ('exp') and Eurocode 3 ('EC3') are provided in Table 1, with the corresponding mean and the coefficient of variation (COV) given in Table 2. Following the general observations made by analysing Fig. 3, three slenderness ranges are considered in Table 2: predictions for all $\bar{\lambda}$, $\bar{\lambda} \leq 1$ and $\bar{\lambda} > 1$.

In Table 2, the good agreement between experimental results and model predictions is underlined by the mean and the COV being 0.975 and 0.101 for all $\bar{\lambda}$ respectively. Excellent results are highlighted for $\bar{\lambda} \leq 1$ with the mean and the COV being 1.033 and 0.075, respectively. As observed by analysing Fig. 3, slightly larger deviations are present for the mean and the COV for $\bar{\lambda} > 1$ (0.906 and 0.082, respectively).

4.3. Comparison with tangent modulus load

The energy formulation provided in Section 2 presents an alternative, non-iterative, method to determine the buckling strength of columns corresponding to the tangent modulus buckling load, *i.e.* the lowest possible bifurcation load of struts undergoing nonlinear (plastic) deformation. Fig. 4 demonstrates that predictions of the current model coincide with tangent modulus buckling loads. Therefore, two strength curves corresponding to hardening parameters $n = \{3, 9\}$ with an elastic modulus of $E = 210\,\text{GPa}$ and a proof stress of $f_y = 450\,\text{MPa}$ are compared against tangent modulus load predictions following the SEI/ASCE-8 standard (iterative method) [3], indicated by circle symbols 'o' in Fig. 4. All tangent modulus buckling load predictions coincide with the results of the current model confirming their equivalence.

4.4. Parametric study

Since the experimental results presented in Fig. 3 correspond to a wide range of material types or grades, a parametric study is performed employing the energy formulation presented in Section 2, which is ideally suited to investigate the effect of changing material parameters on the column strength directly. First, the effect of changing the hardening parameter n is studied in Fig. 5, where experimental data and the Eurocode 3 design curve are also provided. Fig. 5 shows that changing the hardening parameter particularly affects the column strength for smaller $\bar{\lambda}$ values. Increasing n values increase the column strengths for intermediate slendernesses, *i.e.* $\bar{\lambda} = [0.7, 1.8]$, and reduce the column strengths for $\bar{\lambda} < 0.7$.

Changing the proof stress f_y also alters the behaviour of the struts significantly. As illustrated in Fig. 6 for hardening parameters $n = 5$ and $n = 7$, different proof stresses generate a band in strength predictions starting at the normalized slenderness (towards smaller $\bar{\lambda}$) where the response begins to deviate from the Euler load predictions in the range $\bar{\lambda} \approx [1.5, 1.7]$. In Fig. 6, proof stresses in the range of $f_y = [235\,\text{MPa}, 960\,\text{MPa}]$ are considered, deemed to cover a wide range of characteristic material grades used in structural members made from stainless steel.

As indicated by the width of the bands in strength predictions (represented by the gap between the black and magenta lines in Fig. 6),

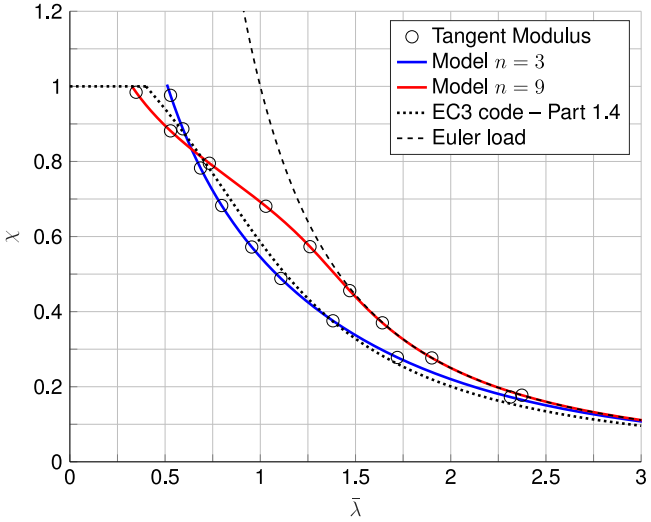

Fig. 4. Comparison with tangent modulus load ($E = 210$ GPa, $f_y = 450$ MPa).

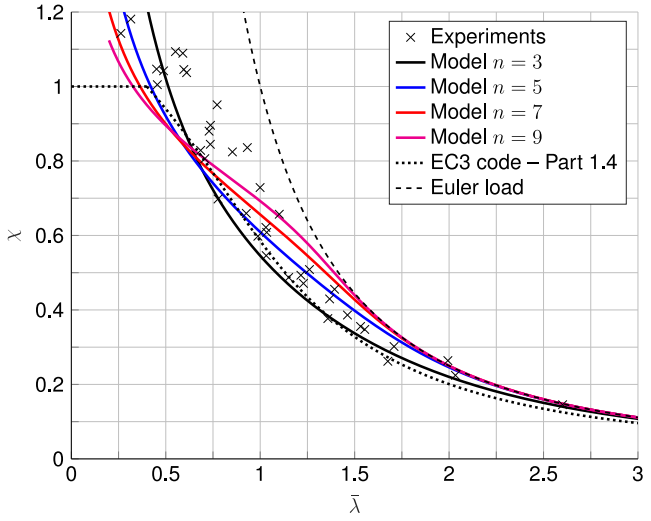

Fig. 5. Effect of varying the hardening parameter n; comparison against experimental data and EC3 design curve; strength reduction factor χ vs. normalized slenderness $\bar{\lambda}$; stainless steel properties used ($E = 210$ GPa, $f_y = 450$ MPa).

increasing proof stresses cause varying increases in strength for different $\bar{\lambda}$ values. The size of such bands is also affected by the hardening parameter n. This can be illustrated by comparing strength predictions in two ways: first, $\bar{\lambda}$ values corresponding to a strength reduction factor of $\chi = 1$, *i.e.* $\bar{\lambda}_0^{\text{m}} \equiv \bar{\lambda}(\chi = 1)$, are evaluated for the largest and lowest proof stress considered (superscript "m" is used to provide a distinction from the measure $\bar{\lambda}_0$ used in the Eurocode design curves, see [2]); second, χ values are evaluated for fixed $\bar{\lambda}$ values.

In Fig. 6(a), for $n = 5$ and $f_y = (235\,\text{MPa}, 960\,\text{MPa})$, the normalized slendernesses corresponding to $\chi = 1$ are $\bar{\lambda}_0^{\text{m}} = (0.32, 0.56)$ which changes for $n = 7$ (Fig. 6(b)) to $\bar{\lambda}^{\text{m}} = (0.27, 0.49)$, indicating the narrowing of the aforementioned band in strength predictions which proceeds with increasing n values. Considering strength predictions for fixed $\bar{\lambda}$, for $n = 5$ and $f_y = 960\,\text{MPa}$ at $\bar{\lambda} = \bar{\lambda}_0^{\text{m}} = 0.56$, a strength of $\chi = 1$ is reached, whereas for $f_y = 235\,\text{MPa}$ the strength reduces to $\chi = 0.77$ for $\bar{\lambda} = 0.56$. For $n = 7$, a strength of $\chi = 1$ is reached at $\bar{\lambda} = \bar{\lambda}_0^{\text{m}} = 0.49$ for $f_y = 960\,\text{MPa}$, whereas for $f_y = 235\,\text{MPa}$ the strength decreases to $\chi = 0.83$ for $\bar{\lambda} = 0.49$.

To highlight the effect of changing the hardening parameter n and the proof stress f_y, Fig. 7 presents strength predictions for configurations that may be regarded as upper and lower bounds for structural

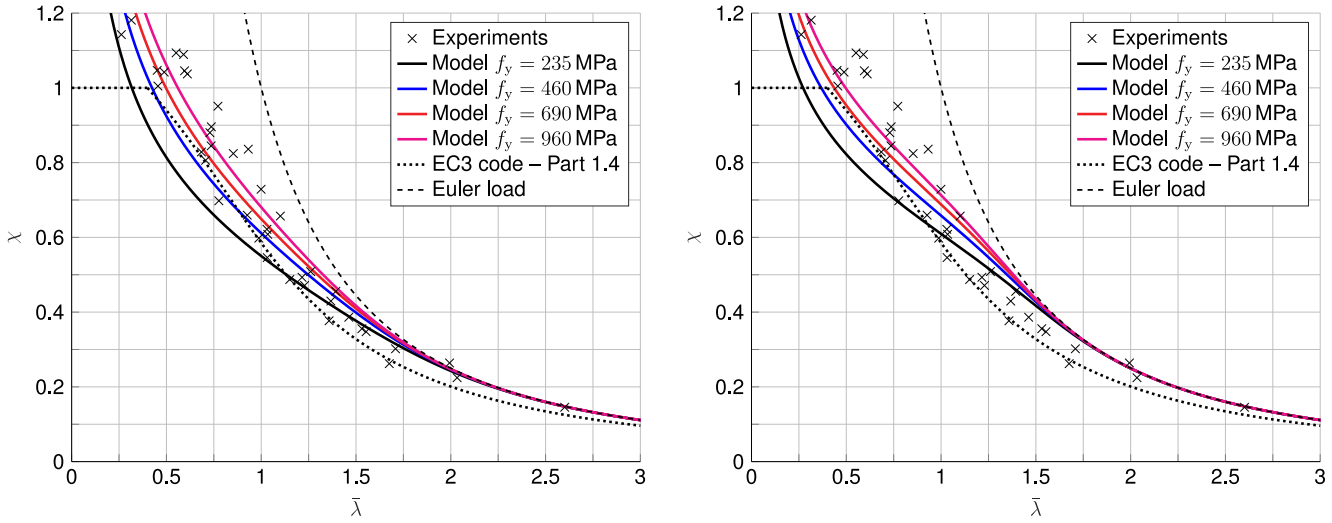

(a) $n = 5$. (b) $n = 7$.

Fig. 6. Effect of varying proof stress f_y for (a) $n = 5$ and (b) $n = 7$; comparison against experimental data and design curve; strength reduction factor χ vs. normalized slenderness $\bar{\lambda}$; stainless steel ($E = 210$ GPa).

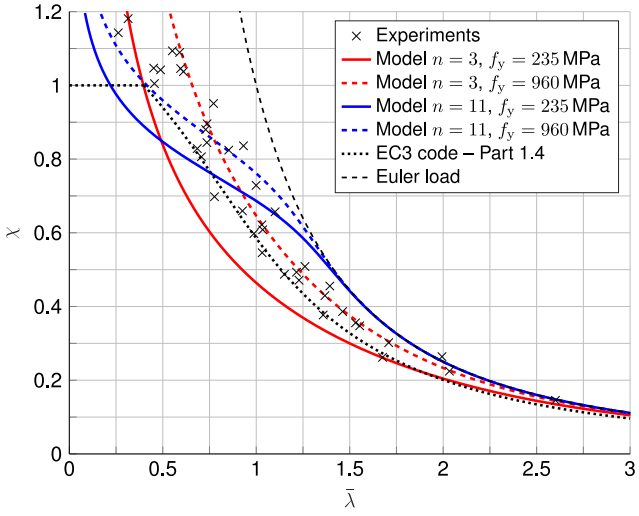

Fig. 7. Comparison of lower and upper bounds for n and f_y.

members made from stainless steel. Therefore, Fig. 7 also serves to visualize the significant deviations between strength predictions of such cases and thus provides an argument towards the need for design recommendations that consider variations in material parameters.

For normalized slendernesses $\bar{\lambda}$ associated with strength predictions $\chi \leq 1$, a comparison between $n = 3$ and $n = 11$ for $f_y = 235$ MPa shows that strength predictions may deviate by up to 36% (at $\bar{\lambda} \approx 1.15$) but coincide at other values of normalized slenderness ($\bar{\lambda} \approx 0.49$). This changes for $f_y = 960$ MPa, where the maximum deviation decreases to 21% (at $\bar{\lambda} \approx 1.18$) with coinciding predictions at $\bar{\lambda} \approx 0.78$. As performed while analysing Fig. 6, ranges of normalized slendernesses associated with $\chi = 1$, *i.e.* $\bar{\lambda}_0^{\mathrm{m}}$, can be evaluated for highlighting the effect of changing material parameters. Fig. 7 shows that $\bar{\lambda}_0^{\mathrm{m}}$ values may range from 0.22 up to 0.66, where these minimum and maximum values are associated with large hardening parameters in conjunction with low proof stresses and small hardening parameters with large proof stresses respectively; these may therefore be regarded as lower and upper bounds respectively.

4.5. New design provision proposal

The results presented in Sections 4.2 to 4.4 demonstrate that the developed buckling load formula provides accurate strength predictions corresponding to the tangent modulus load. The results also indicate that design formulae should consider varying material parameters for predicting the column strength. Based on the comparison against experimental data presented in Section 4.2, a new design recommendation is formulated next.

Excellent agreement of the currently presented model with experimental data has been documented for $\bar{\lambda} \leq 1$ in Tables 1 and 2. On the other hand, the model overestimates the column strength for $\bar{\lambda} > 1$ while exhibiting a small COV. It should be noted that, in its current form, the model does not consider geometric imperfections and residual stresses. The results documented in Section 4.2 indicate that such effects become significant with larger $\bar{\lambda}$, particularly for $\bar{\lambda} > 1$. Without altering the derivation of the buckling load formula, *cf.* Eqs. (16) and (17), the effect of lowering the column strength due to geometric imperfections can be included *a posteriori* in the model by introducing a correction factor β that decreases the roundness (nonlinearity) of the stress–strain behaviour and thus serves to make the structural response of the column smoother, as expected when geometric imperfections would be present. Hence, the correction factor β is assigned to the hardening exponent n, altering the buckling load formula to the following:

$$f(p) = p^{\beta n} + C_1 p + C_2 = 0, \quad \text{with:} \quad C_1 = \frac{1}{(\beta n + 1)c_1}, \quad C_2 = -\frac{c_2}{c_1}, \quad c_2 = \frac{\pi^2 I_{zz}}{(\beta n + 1)AL^2}, \quad c_1 = \frac{\beta n \alpha_{\mathrm{ro}} E^{\beta n}}{(\beta n + 1) f_y^{\beta n}}. \tag{18}$$

The concept of introducing such a correction factor has been demonstrated in [30], where hot-rolled and welded structural members were considered.

The upper bound of β is 1, giving the original model formulation. The lower bound of β is to a certain extent arbitrary; however, values that make the material response linear, *i.e.* $\beta n = 1$, represent a reasonable lower bound. In addition to the assessment that the correction factor appears to be mainly required for larger normalized slendernesses, some physical insights must be considered when introducing a correction factor by means of lowering the hardening exponent, thus:

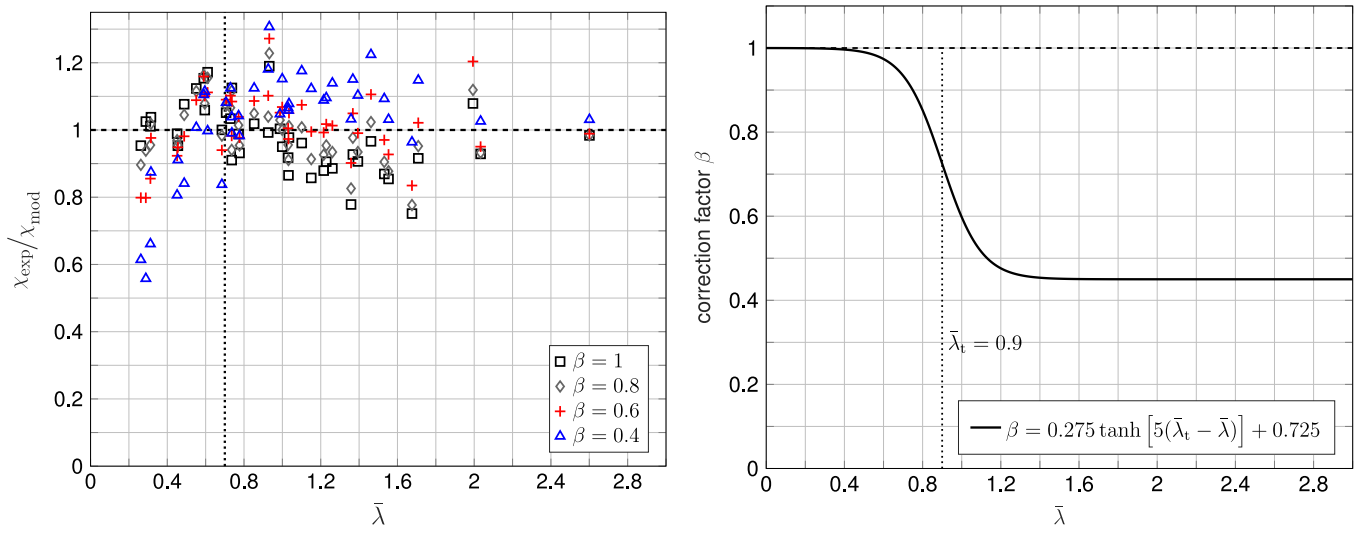

(a) Experiment vs. model for varying β.

(b) Correction factor β vs. $\bar{\lambda}$.

Fig. 8. Analysis of the correction factor β; (a) ratio of the strength reduction factor χ_{exp}/χ_{mod} against normalized slenderness $\bar{\lambda}$, (b) proposed function for $\beta(\bar{\lambda})$.

- Owing to the nonlinearity of the material behaviour, strength curves associated with different hardening parameters intersect each other at intermediate normalized slendernesses; for instance, in the range between 0.6 and 0.7 for the material parameters considered in the comparison against experimental data (*cf.* Fig. 5). Thus, for normalized slendernesses smaller than the value associated with the intersection of the strength curves, the correction factor increases the buckling load. For larger $\bar{\lambda}$ values, the correction factor β represents the strength reduction effect of geometric imperfections. As a consequence, the correction factor should only be applied to configurations associated with normalized slendernesses larger than the value corresponding to the intersection point of respective strength curves with different hardening exponents. This normalized slenderness limit is critical for the implementation of the correction factor and is subsequently referred to as the *transition slenderness* $\bar{\lambda}_t$.
- Despite the aforementioned categorization of where the correction factor should be applied in terms of the normalized slenderness, a representation of the correction factor by means of a continuous function is required. This accounts for the gradually increasing effect of imperfections on the ultimate strength as well as considering that the *transition slenderness* $\bar{\lambda}_t$ does not represent a fixed quantity but rather changes within a certain region of normalized slendernesses depending on the given material parameters.

The aforementioned points are visualized in Fig. 8. The effect of the correction factor on the strength predictions is studied in Fig. 8(a) for β values in the range of 0.4–1.0 by means of the ratio of strength reduction factors (χ) between the experiments (exp) and the model (mod). The proposed continuous representation of the correction factor is provided in Fig. 8(b).

In Fig. 8(a), for the experimental data considered, the transition slenderness $\bar{\lambda}_t$ is approximately 0.7 (dotted vertical line in Fig. 8(a)). All configurations associated with $\bar{\lambda} < \bar{\lambda}_t$ exhibit the aforementioned increase in buckling load when applying the correction factor (lowering the strength reduction ratio). For $\bar{\lambda} \geq \bar{\lambda}_t$, the intended effect of lowering the buckling load (increasing the strength reduction ratio) is obtained. It should also be noted that the effect of the correction factor in the vicinity of $\bar{\lambda}_t$ is small since the corresponding strength curves are close to each other for such $\bar{\lambda}$ values. Moreover, minor deviations in strength predictions are present for β values up to 0.8, whereas significant effects occur for β values smaller than 0.8; see the '+' and '▵' symbols in Fig. 8(a).

The continuous function for the correction factor $\beta(\bar{\lambda})$ shown in Fig. 8(b) aims at providing a generally applicable form. Therefore, a generic $\bar{\lambda}_t$ value must be determined. This can be achieved by identifying an upper bound of such a transition slenderness, since for all $\bar{\lambda} < \bar{\lambda}_t$ the model formulation with the 'original' hardening parameter ($\beta = 1$) gives excellent results. Fig. 7, showing 'extreme' cases of material parameters deemed to relate to stainless steel, visualizes how the upper bound of $\bar{\lambda}_t$ can be determined. Considering a constant Young's modulus E, the intersection point of the strength curves shifts towards larger normalized slendernesses with increasing proof stresses. For $f_y = 960\,\text{MPa}$, the transition slenderness is 0.8. In general, this shift depends on the ratio of proof stress to Young's modulus, *i.e.* $\Delta = f_y/E$, where increasing Δ values increase the value of $\bar{\lambda}_t$.[2] A parametric study on the effect of Δ on $\bar{\lambda}_t$ has been performed also considering changing pairs of hardening parameters. As a result, an upper bound of $\bar{\lambda}_t = 0.9$ has been determined that holds for all types/grades of aluminium alloys and stainless steels used in structural engineering, where ratios of $\Delta \leq 0.01$ have been considered alongside associated ranges of hardening exponents.

Considering the distinct regions identified, marked by the newly introduced transition slenderness $\bar{\lambda}_t$, the correction factor β is expressed as follows:

$$\beta = a_1 \tanh\left[a_0(\bar{\lambda}_t - \bar{\lambda})\right] + a_2, \text{ with: } a_0 = 5,\ a_1 = 0.275,\ a_2 = 0.725, \quad (19)$$

with $\bar{\lambda}_t = 0.9$, which is plotted in Fig. 8(b). The constants a_1 and a_2 ensure that the limits of the tanh-function are unity and the minimal correction factor employed ($\beta_{min} = 0.45$). Moreover, the values of a_1, a_2 and a_3 have been selected to provide the best agreement possible with experimental data in terms of the mean and COV while maintaining generally safe predictions. Note that by describing the correction factor by means of a continuous function, normalized slendernesses smaller than the general value of $\bar{\lambda}_t$ but within its vicinity are assigned a correction factor smaller than 1.0. As aforementioned, the associated effect on the strength predictions is negligible and, thus, does not restrict the applicability of the proposed function.

[2] The pair of distinct hardening parameters considered also affects the transition slenderness $\bar{\lambda}_t$. However, this becomes relevant for determining an upper bound of $\bar{\lambda}_t$ only if both considered hardening exponents are small but cause a qualitative change in the behaviour of the associated strength curves, for instance when considering $n = \{3, 5\}$. This effect is considered in determining the upper bound of $\bar{\lambda}_t$.

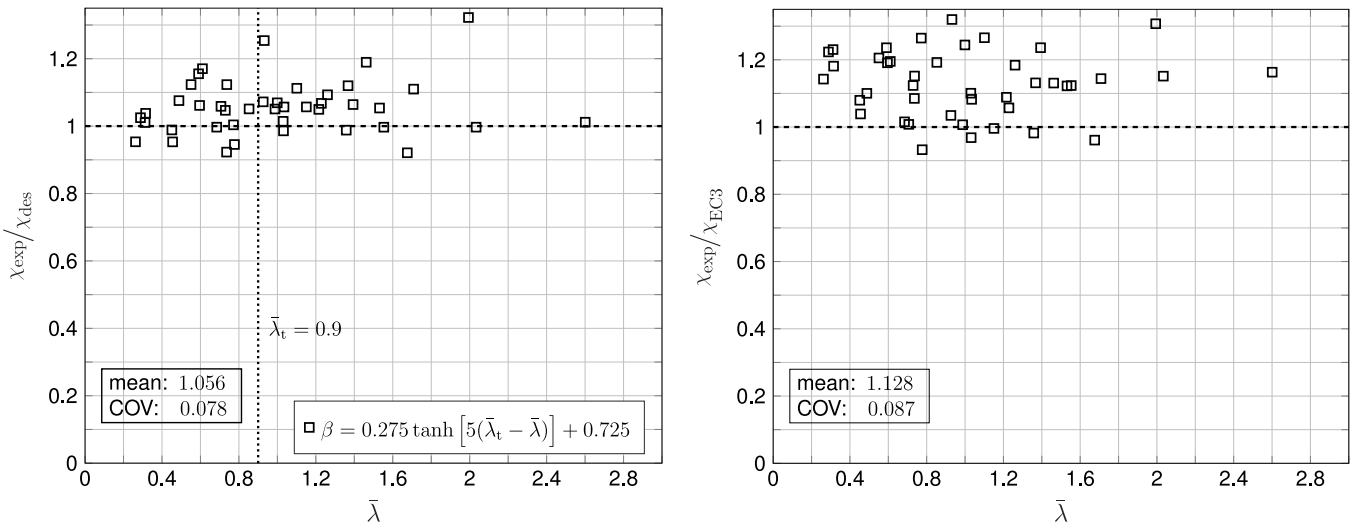

(a) χ_{exp}/χ_{des} vs. $\bar{\lambda}$. (b) χ_{exp}/χ_{EC3} vs. $\bar{\lambda}$

Fig. 9. Design provision: (a) design model predictions, (b) Eurocode predictions.

In summary, the following design proposition is made. The column strength of structural members made from materials following the Ramberg–Osgood constitutive law for which flexural buckling is critical can be accurately predicted solving Eq. (18) with the implementation of the correction factor expressed in Eq. (19), thus:

Eq. (18): $f(p) = 0 \Longrightarrow p^{C}$ with $\beta = \beta(\bar{\lambda})$ in the form of Eq. (19). (20)

Eq. (20) constitutes the governing equation of the proposed design model (des).

The results of the design model are provided in terms of strength ratio (χ_{exp}/χ_{des}) against normalized slenderness ($\bar{\lambda}$) in Fig. 9(a). Corresponding results comparing the Eurocode 3 predictions against the experimental data are shown in Fig. 9(b). The design model exhibits a mean and COV of 1.056 and 0.078 respectively, with Eurocode 3 predictions having a mean and COV of 1.128 and 0.087, respectively.

4.6. Reliability analysis

The reliability analysis, in the form of a First Order Reliability Method, follows the guidelines provided in the Eurocode [31] alongside information provided in [32] to determine the partial safety factor γ_{M1}. The partial safety factor is employed to guarantee that the probability of the resistance of a structural member being below its design resistance does not exceed a certain threshold. Considering the reliability class RC2 (see [31]), this probability is approximately 0.001 [32]. The recommended partial safety factor for stability design in EC3-Part 1.4 is $\gamma_{M1} = 1.1$ [2]. Subsequently, the terminology of the Eurocode is adopted, thus a strength value obtained from the proposed model and experiments are denoted by r_t and r_e, respectively. Note that single data points are denoted with a superscript i.

To obtain the coefficient of variation of the model errors (V_δ), first, the least-squares best fit to the data, denoted by the parameter b, is determined, thus:

$$b = \frac{\sum_{i=1}^{n} r_t^i r_e^i}{\sum_{i=1}^{n} \left(r_e^i\right)^2}. \tag{21}$$

Fig. 10(a) shows the data points $\{r_t^i, r_e^i\}$ for all n experiments considered ($i = \{1, 2, \ldots, n\}$) alongside the corresponding reference line for $r_t^i = r_e^i$. The b-factor is applied to the predictions of the model for all data points resulting in the scatter diagram shown in Fig. 10(b).

With the b-factor, the relative error δ^i of the model predictions for each data point is determined, *i.e.* $\delta^i = r_e^i/(b r_t^i)$. Next, the logarithm of the error terms, *i.e.* $\Delta^i = \log\left(\delta^i\right)$, is calculated followed by determining

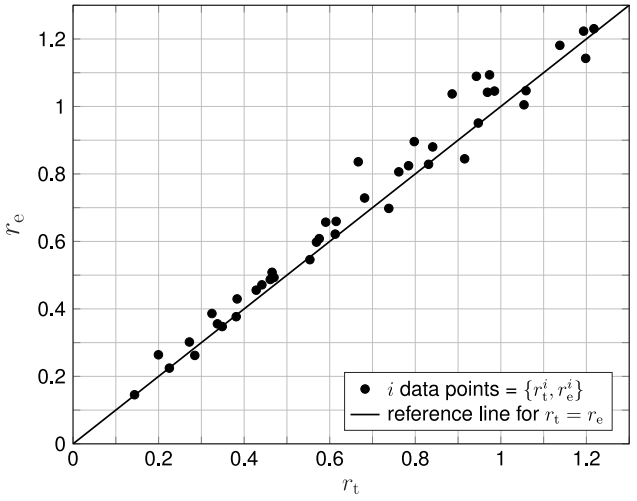

(a) data points $\{r_t^i, r_e^i\}$.

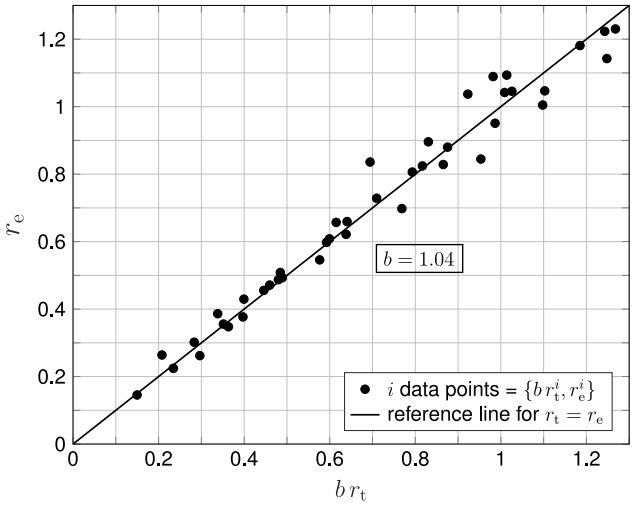

(b) data points $\{b\, r_t^i, r_e^i\}$.

Fig. 10. Scatter diagrams comparing theoretical (r_t) and experimental (r_e) strength predictions; (a) without and (b) with the b-factor.

Table 3
Mean and coefficient of variation (COV) of basic variables X_j taken from [32,33].

	Mean	COV
f_y	$f_{y,m} = 1.1 f_{y,n}$ for duplex	0.030
	$f_{y,m} = 1.2 f_{y,n}$ for ferritic	0.045
E	$E_m = E_n$	0.030
A	$A_m = A_n$	0.030

the respective mean, *i.e.* $\bar{\Delta} = \left(\sum_{i=1}^{n} \Delta^i\right)/n$. The variance of Δ^i, denoted by s_Δ^2, being the estimated value of the variance of the logarithmic error σ_Δ^2, is determined by

$$s_\Delta^2 = \frac{1}{n-1} \sum_{i=1}^{n} \left(\Delta^i - \bar{\Delta}\right)^2. \tag{22}$$

With s_Δ^2 determined, the coefficient of variation of the error terms δ^i is calculated by

$$V_\delta = \sqrt{\exp\left(s_\Delta^2\right) - 1}, \tag{23}$$

providing a measure for the variability of the proposed design model predictions. A value of $V_\delta = 0.076$ has been determined.

The variability of the basic variables entering the resistance function (proposed design model) is determined next. The basic variables are the proof stress f_y, the Young's modulus E and the cross-sectional area A, which are denoted by X_j. The corresponding coefficient of variation V_{rt} is calculated by

$$V_{rt}^{i\,2} = \frac{1}{r_t^i(\underline{X}_m)^2} \sum_{j=1}^{k} \left(\frac{\partial r_t^i}{\partial X_j} \sigma_j\right)^2, \tag{24}$$

where $\underline{X}_m$ is the array of the mean values of the basic variables and σ_j is the standard deviation of the jth basic variable [32,33]. The mean values and coefficients of variation (COV) of the basic variables are provided in Table 3, where a subscript 'n' refers to the nominal values. The partial derivatives in Eq. (24) are determined numerically. Note that V_{rt} is calculated for each data point. To provide a general estimate, a mean of $V_{rt} = 0.029$ has been determined. With Eq. (24), the resultant of the coefficients of variation V_r can be determined for each data point by

$$V_r^{i\,2} = V_{rt}^{i\,2} + V_\delta^2, \tag{25}$$

and taking the square root, where V_δ has been determined using Eq. (23) and remains unchanged. A mean of $V_r = 0.082$ has been determined.

In the final step, the design resistance r_d is calculated for each data point, thus:

$$r_d^i = b\, r_t^i(\underline{X}_m) \exp(-k_{d,\infty}\alpha_{rt}^i Q_{rt}^i - k_{d,n}\alpha_\delta^i Q_\delta^i - 0.5 Q^{i\,2}), \tag{26}$$

with $k_{d,\infty} = k_{d,n} = 3.04$ since a sufficiently large number of data points are considered [31,32]. The remaining parameters are given by

$$\begin{aligned} Q_{rt}^i &= \sqrt{\log\left(V_{rt}^{i\,2} + 1\right)}, \quad Q_{rt}^i = \sqrt{\log\left(V_\delta^{i\,2} + 1\right)}, \\ Q_{rt}^i &= \sqrt{\log\left(V_r^{i\,2} + 1\right)}, \\ \alpha_{rt}^i &= Q_{rt}^i/Q^i, \qquad \alpha_\delta^i = Q_\delta^i/Q^i. \end{aligned} \tag{27}$$

Note that $r_t^i(\underline{X}_m)$ are the strength predictions obtained by the proposed model considering the measured basic variables in the respective experimental studies [13,28,29]. With Eq. (26), the required partial safety factor γ_{M1}^* can be calculated for each data point, thus:

$$\gamma_{M1}^{*i} = \frac{r_n^i}{r_d^i}, \tag{28}$$

where r_n^i (or sometimes referred to as characteristic resistance r_k^i) is the nominal resistance using the nominal values for the basic variables in the proposed resistance function (*cf.* Table 3). Determining the least-square best fit gives the partial safety factor of the novel design provision. A value of $\gamma_{M1}^* = 1.10$ has been determined that matches the current recommended partial resistance factor stated in the Eurocode.

It should be noted that the proposed design provision and thus the resistance function evaluated employs a function for the correction factor that is deemed to be generally applicable to Ramberg–Osgood materials (*cf.* Eq. (19) and Fig. 9(a)), where further reductions of the partial safety factor may be achievable by optimizing the correction factor function for material types and grades, if deemed necessary.

5. Conclusions

With the aid of a novel simplified energy formulation employing the total potential energy principle, a governing equation for struts made from materials obeying the Ramberg–Osgood law (*e.g.* stainless steel, cold-formed steel, aluminium alloys) with arbitrary cross-sections and for any slendernesses for which flexural buckling is critical is derived. The formula solely depends on the material parameters Young's modulus E, hardening exponent n and proof stress f_y, alongside the strut slenderness λ. Buckling loads may be readily obtained by simple numerical solution methods, built-in root evaluation functions in algebraic manipulation software or spreadsheet software, where a closed-form solution exists for $n = 3$ (see Appendix). The model represents a non-iterative alternative to the design load employing the tangent modulus approach. Finite element simulations and comparisons with experimental data verify the proposed model.

The model facilitates direct and comprehensive parametric studies on the effect of material and geometric parameters on the compressive strength of struts. The study demonstrates that strength predictions alter significantly (quantitatively and qualitatively) with changing material parameters such as the hardening exponent and the proof stress. This highlights that either material parameters should enter design recommendations directly or the effect of changing parameters should be considered (for instance for specific material grades/types).

A design model is developed that incorporates a correction factor in the form of lowering the hardening exponent – considered to represent the effect of imperfections – within the energy formulation. Owing to the comprehensive parametric study performed, a physically sound implementation of the correction factor by means of a continuous function of the normalized slenderness is proposed. Therefore, the parameter 'transition slenderness' is introduced; the transition marks the minimum normalized slenderness from where the correction factor accounts for the effect of imperfections on the structural responses. The introduction of the proposed correction factor effectively resolves the inherent weakness of the tangent modulus design load, *i.e.* overestimating the column strength for larger normalized slendernesses.

The design model provides excellent agreement with experimental data. This is underlined by evaluating the ratio of strength reduction factors between experiments and the design model where a mean and coefficient of variation (COV) of 1.056 and 0.078 is obtained, respectively. The results represent an improvement in relation to predictions from the Eurocode 3 (mean: 1.128, COV: 0.087). Moreover, reliability requirements specified in the structural Eurocodes are met by the novel design model.

Declaration of competing interest

The authors declare that they have no known competing financial interests or personal relationships that could have appeared to influence the work reported in this paper.

Appendix. Closed-form solution for $n = 3$

The governing equation in Eq. (16) can be solved in closed-form for a hardening exponent of $n = 3$. Inserting $n = 3$ in Eq. (16) gives the following solution for the non-dimensional buckling load p^c, thus:

$$p^C = \frac{\left(\sqrt{3\left(27\,C_2^2 + 4\,C_1^3\right)} - 9\,C_2\right)^{1/3}}{2^{1/3}\,3^{2/3}} - \frac{\left(\frac{2}{3}\right)^{1/3} C_1}{\left(\sqrt{3\left(27\,C_2^2 + 4\,C_1^3\right)} - 9\,C_2\right)^{1/3}} \tag{A.1}$$

with the buckling load being simply $P^C = p^C E A$, where the coefficients C_1 and C_2 are provided in Eq. (16).

References

[1] Gardner L. Stability and design of stainless steel structures – Review and outlook. Thin-Walled Struct 2019;141:208–16.
[2] European Committee for Standardisation (CEN). Design of steel structures: part 1-4: general rules: supplementary rules for stainless steel. Eurocode 3, EN 1993-1-4, Brussels, Belgium; 2010.
[3] American Society of Civil Engineers. Specification for the design of cold-formed stainless steel structural members. SEI/ASCE 8-02, Reston, Virginia, USA; 2002.
[4] Trahair NS, Bradford MA, Nethercot DA, Gardner L. The behaviour and design of steel structures to EC3. fourth ed.. Taylor and Francis; 2008.
[5] European Committee for Standardisation (CEN). Design of steel structures: part 1-1: general rules and rules for buildings. Eurocode 3, EN 1993-1-1, Brussels, Belgium; 2010.
[6] Ban H, Shi G, Shi Y, Wang Y. Overall buckling behavior of 460 MPa high strength steel columns: Experimental investigation and design method. J Constr Steel Res 2012;74:140–50.
[7] Ban H, Shi G, Shi Y, Bradford M. Experimental investigation of the overall buckling behaviour of 960 MPa high strength steel columns. J Constr Steel Res 2013;88:256–66.
[8] Meng X, Gardner L. Behavior and design of normal and high strength steel SHS and RHS columns. J Struct Eng 2020;146(11):04020227.
[9] Ramberg W, Osgood WR. Description of stress–strain curves by three parameters. Technical note (902), Washington, D.C. USA; 1943.
[10] Arrayago I, Real E, Gardner L. Description of stress–strain curves for stainless steel alloys. Mater Des 2015;87:540–52.
[11] Yun X, Wang Z, Gardner L. Full-range stress–strain curves for aluminum alloys. J Struct Eng 2021;147(6):04021060.
[12] Rasmussen KJR, Rondal J. Strength curves for metal columns. J Struct Eng 1997;123(6):721–8.
[13] Huang Y, Young B. Tests of pin-ended cold-formed lean duplex stainless steel columns. J Constr Steel Res 2013;82:203–15.
[14] Arrayago I, Rasmussen KJR. Buckling curves for cold-formed stainless-steel columns and beams. J Struct Eng 2021;147(10):04021149.
[15] Chen L, Yu Y, Song W, Wang T, Sun W. Stability of geometrically imperfect struts with Ramberg–Osgood constitutive law. Thin-Walled Struct 2022;177:109438.
[16] Chen L, Yu Y, Cheng J, Zheng S, Lim CW. Accurate analytical approximation to post-buckling of column with Ramberg–Osgood constitutive law. Appl Math Model 2021;98:121–33.
[17] Szymczak C, Kujawa M. Flexural buckling and post-buckling of columns made of aluminium alloy. Eur J Mech A Solids 2019;73:420–9.
[18] Szymczak C, Kujawa M. Buckling of thin-walled columns accounting for initial geometrical imperfections. Int J Non-Linear Mech 2017;95:1–9.
[19] Standards Australia. Cold-formed stainless steel structures. AS/NZS 4673, Sydney, AUS; 2001.
[20] Thompson JMT, Hunt GW. A general theory of elastic stability. London: John Wiley & Sons; 1973.
[21] Thompson JMT, Hunt GW. Elastic instability phenomena. Chichester: John Wiley & Sons; 1984.
[22] Bai L, Wadee MA, Köllner A, Yang J. Variational modelling of local–global mode interaction in long rectangular hollow section struts with Ramberg–Osgood type material nonlinearity. Int J Mech Sci 2021;209:106691.
[23] Hunt GW, Da Silva LS, Manzocchi GME. Interactive buckling in sandwich structures. Proc R Soc A 1988;417(1852):155–77.
[24] Shanley FR. Inelastic column theory. J Aeronaut Sci 1947;14:261–7.
[25] Hutchinson JW. Plastic buckling. Adv Appl Mech 1974;14:67–144.
[26] Abaqus. ABAQUS/Standard. Providence RI, USA: Dassault Systèmes; 2019.
[27] European Committee for Standardisation (CEN). Design of steel structures: part 1-4: plated structural elements. Eurocode 3, EN 1993-1-5, Brussels, Belgium; 2010.
[28] Theofanous M, Gardner L. Testing and numerical modelling of lean duplex stainless steel hollow section columns. Eng Struct 2009;31:3047–58.
[29] Afshan S, Gardner L. Experimental study of cold-formed ferritic stainless steel hollow sections. J Struct Eng 2013;139(5):717–28.
[30] Walport F, Kucukler M, Gardner L. Stability design of stainless steel structures. J Struct Eng 2022;148(1):04021225.
[31] European Committee for Standardisation (CEN). Eurocode – basis of structural design. Eurocode, EN 1990:2002+A1:2005, Brussels, Belgium; 2010.
[32] Afshan S, Francis P, Baddoo NR, Gardner L. Reliability analysis of structural stainless steel design provisions. J Constr Steel Res 2015;114:293–304.
[33] Behzadi-Sofiani B, Gardner L, Wadee MA. Stability and design of fixed-ended stainless steel equal-leg angle section compression members. Eng Struct 2021;249:113281.